

Quasi-Monte Carlo Algorithms (not only) for Graphics Software

Alexander Keller, Carsten Wächter, and Nikolaus Binder

Abstract Quasi-Monte Carlo methods have become the industry standard in computer graphics. For that purpose, efficient algorithms for low discrepancy sequences are discussed. In addition, numerical pitfalls encountered in practice are revealed. We then take a look at massively parallel quasi-Monte Carlo integro-approximation for image synthesis by light transport simulation. Beyond superior uniformity, low discrepancy points may be optimized with respect to additional criteria, such as noise characteristics at low sampling rates or the quality of low-dimensional projections.

Key words: Quasi-Monte Carlo methods · Low discrepancy sequences · Software · Parallel algorithms

1 Introduction

Physically based image synthesis [41] consists of computing pixel colors as functionals of the solution of a Fredholm integral equation that models light transport. The simulations are based on sampling light transport paths and summing up their contributions. In early computer graphics, Monte Carlo methods using random samples have been applied. Today, quasi-Monte Carlo methods have become the industry standard [22] and are an active domain of research [24].

There are several reasons for this development. First of all, the points of low discrepancy sequences as used for sampling in quasi-Monte Carlo methods are much more uniformly distributed than random numbers ever can be [36], which improves efficiency. In addition, deterministic low discrepancy sequences allow for reproducible and massively parallel computation without the risk of inefficiencies. In fact, their extensibility lends itself to progressive, adaptive, and consistent algorithms.

Alexander Keller e-mail: akeller@nvidia.com · Carsten Wächter e-mail: cwachter@nvidia.com · Nikolaus Binder e-mail: nbinder@nvidia.com
NVIDIA, Fasanenstr. 81, 10623 Berlin, Germany

In the following, efficient implementations of sampling algorithms for quasi-Monte Carlo methods as used in industry are presented and discussed. For the example of photorealistic image synthesis, which amounts to numerical integro-approximation computing millions of integrals in parallel, a new sampling scheme is proposed. The simple algorithm excels at visual quality, especially at low sampling rates and hence is a perfect candidate for real-time light transport simulation.

2 Implementation of Low Discrepancy Sequences

Digital (t, s) -sequences and rank-1 lattice sequences are the two most popular approaches to generate low discrepancy sequences. While implementations may seem straightforward, there are several practical issues that deserve attention.

Today’s speed of computing is dominated by the cost of moving data rather than the cost of arithmetic operations. Hence, replacing memory accesses by computations may be more efficient than a table lookup. Yet, a smaller code size and more efficient code may result from the use of the lookup tables. Balancing these competing goals, both data and code will remain in the respective processor caches, which may dramatically improve performance.

2.1 Floating Point Conversion

Although constructed over finite fields, low discrepancy sequences are points in the s -dimensional unit cube $[0, 1)^s$ whose components are represented by floating point numbers [10]. Note that the set of floating point numbers in the unit interval $[0, 1)$ is not uniformly distributed. Due to the representation by a mantissa and an exponent, floating point numbers are more uniformly distributed the closer they are to zero. Collisions are another consequence of this representation. For example, mapping integers to the unit interval by dividing by the maximum value of their range will ultimately result in cases where different integers become mapped to the same floating point number.

Another issue is that type conversion and rounding may yield floating point numbers outside the unit interval. For example, converting a double precision floating point number close to one in the unit interval to single precision may result in a one. This in turn may cause errors in applications that rely on the right-open unit interval $[0, 1)$, where one is excluded, for example, computing the logarithm $\log(1 - x)$ of a component x of a low discrepancy sequence.

To reduce cancellation when adding floating point numbers of sufficiently different magnitudes, computations should remain in integers or finite fields as long as possible, including randomization methods like scrambling and Cranley-Patterson-rotations [37]. For that purpose, the function `map_u32_to_float` in Algorithm 1 maps a uniformly distributed integer $u \in [0, 2^{32})$ to the best 32-bit floating point

representation in the half-open interval $[0, 1)$. It avoids precision issues of a division-based mapping by explicitly setting bits to appropriate values and is inspired by the concepts found in [3, 42]. Counting the number of leading zeros determines the smallest power of two B that is greater than the unsigned integer input u . This upper bound defines the exponent e of the floating point number as $B = 2^e$. For IEEE 754 32-bit floating point numbers with an 8-bit exponent, the bias of the exponent is $2^7 - 1 = 127$. Incorporating this bias, for z leading zeros of the input value the exponent for the target interval becomes $126 - z$. For architectures on which counting the number of leading zeros of zero is either undefined or does not result in 32, we introduce a special case and map zero explicitly to zero, which in addition avoids that zero is mapped to the smallest possible floating point number. We also add a special case for an input value of one, for which the algorithm would shift left by 32 bits. A left shift by the number of bits of the type is undefined behavior according to the C++ standard¹. The leading one of the mantissa of IEEE 754 floating point numbers is implicit. Therefore, we first remove all leading zeros and the highest bit set of our input value. The result is then shifted right by 9 bits so that the mantissa occupies the lowest 23 bits. Placing the 8-bit exponent in the bits 24 to 31 (counting up from the least significant bit) by shifting it left by 23 bits finalizes the mapping. The sign bit in the position of the most significant bit is always zero. Comparing the difference between the mapped values and a reference computed with 64-bit precision for all possible 32-bit floating point values confirms that the implementation is indeed optimal for 32 bits.

Note that for all floating point numbers $\geq \frac{1}{256}$ there will be collisions, i.e. multiple integers mapping to the same floating point number. There is no way around that due to the logarithmic spacing of the floating point numbers.

2.2 Efficient Radical Inversion

Radical inversion is at the core of most popular low discrepancy sequences such as the family of Halton, digital (t, s) -, and rank-1 lattice sequences. A radical inverse is computed by the mapping

$$\mathbb{N}_0 \rightarrow [0, 1) \cap \mathbb{Q}$$

$$i = \sum_{k=0}^{\infty} a_k(i)b^k \mapsto \phi_{b,\sigma}(i) = \sum_{k=0}^{\infty} \sigma_b(a_k(i))b^{-k-1},$$

where an index i is represented by its digits a_k in base b and then these digits are mirrored at the decimal point. The resulting sequence of rational numbers in the right-open unit interval is of low discrepancy [36]. σ_b is a permutation on the range of a digit. If σ_b is the identity, we will use the shorthand ϕ_b .

¹ https://en.cppreference.com/w/cpp/language/operator_arithmetic

Algorithm 1: Routine to optimally map integers in $[0, 2^{32})$ to the unit interval $[0, 1)$ and basic radical inversion. The table `primes` stores the prime numbers and `max_powers` stores the largest prime power that still fits into 32 bits.

```

float map_u32_to_unifloat(uint32_t u)
{
    if (u == 0)
        return 0.f; // snap to 0
    if (u == 1u)
        return __uint_as_float((126-31)<<23);
    uint32_t z = __clz(u); // count leading zeros
    // z is <= 30, as u=0 and u=1 already checked
    uint32_t e = 126-z; // biased exponent
    uint32_t m = (u << (z+1)) >> 9; // discard leading
    // zeroes and first set bit (if any) and
    // shift significant bits into place
    return __uint_as_float((e << 23) | m); // assemble fp32
}

float radinv(uint32_t i, const uint32_t prime_idx)
// allows for full index range [0..0xFFFFFFFF]
{
    const uint32_t base = primes[prime_idx];
    i %= max_powers[prime_idx]; // limit domain
    uint32_t base_tmp = 1;
    uint32_t result = 0;

    do {
        result = result*base + i % base;
        i /= base;
        base_tmp *= base;
    } while(i);

    return map_u32_to_unifloat((uint32_t)
        (((uint64_t) result<<32) / base_tmp));
}

```

Algorithm 1 computes in integers as long as possible and only converts into floating point as a last step. This rules out any cancellation effects due to floating point summation. For efficiency, the index i is limited to the largest prime power that still fits into 32 bits. These values are stored in the table `max_powers`, one for each prime base.

Especially the uniformity of low-dimensional projections of low discrepancy sequences based on radical inverses can be improved by applying permutations σ_b [4, 5] (also known as “digit scrambling”) during radical inversion. The routine `radinv_linscramble` in Algorithm 2 exemplifies computational scrambling by a linear transformation [5]. Note how the implementation prevents overflows of integer multiplications.

Small lookup tables can serve both the purpose of storing arbitrary permutations σ_b and more efficient simultaneous inversion of multiple digits [26] (see Algorithm 2 for the example of ϕ_3). This is illustrated for the recursively defined permutations introduced by Faure [4]: For even b , σ_b is $2\sigma_{\frac{b}{2}}$ concatenated with $2\sigma_{\frac{b}{2}} + 1$. Otherwise, σ_b is σ_{b-1} , where each value $\geq \frac{b-1}{2}$ is incremented by 1 and $\frac{b-1}{2}$ is inserted in the middle. The recursion ends at $\sigma_2 := (0, 1)$. For example, $\sigma_5 = (0, 3, 2, 1, 4)$. In order to compute the radical inversion for two digits, the isomorphism

$$\sigma_5 \times \sigma_5 = \begin{pmatrix} (0, 0) & (0, 3) & (0, 2) & (0, 1) & (0, 4) \\ (3, 0) & (3, 3) & (3, 2) & (3, 1) & (3, 4) \\ (2, 0) & (2, 3) & (2, 2) & (2, 1) & (2, 4) \\ (1, 0) & (1, 3) & (1, 2) & (1, 1) & (1, 4) \\ (4, 0) & (4, 3) & (4, 2) & (4, 1) & (4, 4) \end{pmatrix} \cong \begin{pmatrix} 0 & 3 & 2 & 1 & 4 \\ 25 & 28 & 27 & 26 & 29 \\ 10 & 13 & 12 & 11 & 14 \\ 5 & 8 & 7 & 6 & 9 \\ 20 & 23 & 22 & 21 & 24 \end{pmatrix}$$

is used and tabulated². The loop for radical inversion then performs computations in base b^2 , requiring only half the number of iterations. It is straightforward to extend the principle to more digits. As the size of the lookup table grows exponentially in the number of digits, this approach pays off only for a moderate number of digits and is not efficient once the lookup tables do not stay in the processor caches. Unless the total number of digits to be inverted is a multiple of the digits inverted simultaneously, the remaining digits will have to be inverted individually.

Loop unrolling is an extreme optimization yielding branchless code, which becomes possible by the intrinsically limited number of iterations of radical inversion. The efficiency of loop unrolling varies according to code size and application as it may cool the instruction cache. Unless already done by the compiler, costly division and modulo operations may be replaced by cheaper multiplications, shifts, additions, and subtractions [43].

2.3 Digital Nets and Sequences

The algorithm

$$x_i^{(j)} = \begin{pmatrix} b^{-1} \\ \vdots \\ b^{-m} \end{pmatrix}^T \cdot C_j \cdot \underbrace{\begin{pmatrix} a_0(i) \\ \vdots \\ a_{m-1}(i) \end{pmatrix}}_{\text{multiplication in } \mathbb{F}_b} \in [0, 1) \quad (1)$$

for digital nets and sequences [36] of low discrepancy has the advantage that once implemented, its generator matrices C_j may be replaced by optimized variants (see Sec. 2.6).

Algorithm 3 implements the Sobol' sequence [20, 18, 19], which is the most popular (t, s) -sequence in base $b = 2$. The j -th coordinate $x_i^{(j)}$ is computed by

² Code for the generation of such tables is found at <https://gruenschloss.org>.

Algorithm 2: Examples of linear digit scrambling and simultaneous multiple-digit radical inversion.

```

float radinv_linscramble(uint32_t i, const uint32_t prime_idx)
{
    const uint32_t base = primes[prime_idx];
    const uint32_t scramble = permTN2[prime_idx];
    i %= max_powers[prime_idx];
    uint32_t base_tmp = 1;
    uint32_t result = 0;
    uint32_t im = i % base; // to avoid scramble*im overflow

    do {
        result = result*base + (scramble*im) % base;
        // im % base not required, as im < 0xFFFFFFFF/scramble
        // because base is always > scramble by definition
        i /= base;
        im = i;
        base_tmp *= base;
    } while(i);

    return map_u32_to_unifloat((uint32_t)
        (((uint64_t) result<<32) / base_tmp));
}

float radinv3(uint32_t i)
{
    const unsigned char radinv3_perm[] = {0,3,6,1,4,7,2,5,8};
    i %= 3486784401u; // max_powers
    uint32_t base_tmp = 1;
    uint32_t result = 0;

    do { // two digits at once, hence base 9 = 3 x 3
        result = result*9 + radinv3_perm[i % 9];
        i /= 9;
        base_tmp *= 9;
    } while(i);

    return map_u32_to_unifloat((uint32_t)
        (((uint64_t) result<<32) / base_tmp));
}

```

loading 4 columns of the generator matrix C_j at once to perfectly match a memory interface that fetches 128 bits simultaneously. Each row is masked according to the corresponding bit of the index i and the result is the bit-wise xor (vector arithmetic in \mathbb{F}_2) of all included columns, computing 4 digits simultaneously. The generator matrices are stored for 23 bits of floating point precision, but allow for up to $m = 64$ bit indices in order to enable large numbers of samples. The bits beyond the least significant 32 bits of the index i are determined in the second part of the code

Algorithm 3: CUDA C++ implementation of a selected component of the i -th point of a Sobol' sequence. The generator matrices are stored in `sobol_table` with 23 bits of precision, while 64 bits are used for the index i to enable large numbers of samples. `0xFFFFFFFFu` means that all 64 bits are set.

```
float sobol(uint2 i, const uint32_t j, uint32_t scramble = 0)
{
    const uint32_t adr = j*(52/4);

    for (uint32_t c = 0; (i.x != 0); i.x>>=4, ++c) {
        const uint4 matrix = sobol_table[adr + c];
        scramble ^= ((matrix.x&((i.x & 1) ? 0xFFFFFFFFu : 0))
                    ^ (matrix.y&((i.x & 2) ? 0xFFFFFFFFu : 0)))
                    ^ ((matrix.z&((i.x & 4) ? 0xFFFFFFFFu : 0))
                    ^ (matrix.w&((i.x & 8) ? 0xFFFFFFFFu : 0)));
    }

    i.y &= 0xFFFFu; // only first 20 bits can be looked up,
                  // overall 52bits=32+20

    for (uint32_t c = 8; (i.y != 0); i.y>>=4, ++c) {
        const uint4 matrix = sobol_table[adr + c];
        scramble ^= ((matrix.x&((i.y & 1) ? 0xFFFFFFFFu : 0))
                    ^ (matrix.y&((i.y & 2) ? 0xFFFFFFFFu : 0)))
                    ^ ((matrix.z&((i.y & 4) ? 0xFFFFFFFFu : 0))
                    ^ (matrix.w&((i.y & 8) ? 0xFFFFFFFFu : 0)));
    }

    return map_u32_to_unifloat(scramble);
}
```

example. The integer result then needs to be mapped to floating point as described in Sec. 2.1. Since the result is solely computed by xor operations, digit scrambling can be trivially realized by initializing the parameter `scramble` with a random integer rather than with zero.

2.4 Rank-1 Lattice Sequences

Given a radical inverse $\phi_b(i)$ and a generator vector $\mathbf{g} = (g_0, \dots, g_{s-1})$, whose components $g_j =_b \dots g_{j,3}g_{j,2}g_{j,1}g_{j,0}$ are infinite sequences of digits $g_{j,k} \in \{0, \dots, b-1\}$, a rank-1 lattice sequence [34, 14, 35] consists of the points

$$\mathbf{x}_i = (\phi_b(i) \cdot \mathbf{g}) \bmod [0, 1]^s \quad (2)$$

that will be uniformly distributed if the g_j are linearly independent over the rational integers [34, Thm. 3.1.3, p. 81].

As in practical applications the number of samples ultimately is finite, the required least significant digits of the g_j may be represented by integers, yielding a fast and simple algorithm for generating deterministic uniformly distributed points.

2.4.1 Admissible Generator Vectors in Base $b = 2$

We recollect properties of admissible generator vectors (also see [23, Sec.2.1]): Selecting the components g_j co-prime to the basis b , each dimension is perfectly stratified whenever the number of points is a power of b . The corresponding lattice then is a Latin hypercube sample, similar to the construction of the Sobol' sequence. In Algorithm 4, where $b = 2$, Latin hypercube samples result from odd g_j for 2^m points.

If the components of the generator vector are not unique, there will exist dimensions that are sampled identically instead of uniformly. However, uniqueness is not sufficient, because for b^m points, the components may be identical modulo b^m . The issue is intrinsic to the construction of rank-1 lattice sequences and in [23] has been addressed by requiring the components $g_j \bmod b^m$ to be unique for $0 \leq j < b^m$ and any $m \in \mathbb{N}$. This underlines why the components g_j need to be b -adic integers, as otherwise there exists a number b^m of points from which on components coincide. In practice, where the g_j are represented by integers and the number of samples remains finite, these integers must hence be chosen as large as possible.

Even if the previous constraint is fulfilled, components may be identical modulo b^m , because $g_j \bmod b^m$ generates the same coordinates as $b^m - (g_j \bmod b^m)$. Similar to before, avoiding this symmetry is possible for the first b^{m-1} components $g_j \bmod b^m$ and $m \in \mathbb{N}$. However, once fulfilled for the first b^{m-1} components, it cannot be fulfilled modulo $b^{m'}$ for any $m' < m$. Avoiding the issue completely requires generator components of the form $g_j = 2 \cdot 2^j + 1$, which in turn means that the g_j and the number of points must grow exponentially with dimension.

And yet there remains a flaw: As only the first some least significant digits of the lower dimensions are inspected, for large numbers of points, the more significant digits of the first some generator vector components have never been inspected: While the construction of a uniform rank-1 lattice sequence by primitive polynomials [23] in base $b = 2$ yields unique generator vector components, uniformity still may not be optimal for certain combinations of number of points and dimensions.

One reason for temporarily compromised uniformity are numbers $g_j \bmod b^m$ that are small as compared to b^m . This can be seen by rewriting the rank-1 lattice sequence in (2) as sequence of shifted rank-1 lattices $\mathbf{x}_{kb^m}, \dots, \mathbf{x}_{(k+1)b^m-1}$, $k \in \mathbb{N}_0$, where

$$\phi_b(i + kb^m) \cdot \mathbf{g} = (\phi_b(i) + \phi_b(kb^m)) \cdot \mathbf{g} = \phi_b(i) \cdot \mathbf{g} + \underbrace{\phi_b(k)b^{-m-1}\mathbf{g}}_{=:\Delta_k}$$

for $0 \leq i < b^m$. The shifts Δ_k , who themselves are a rank-1 lattice sequence, are tiny when the components of $\mathbf{g} \bmod b^m$ are small as compared to b^m . As a consequence, the shifted lattices only slowly will fill up the unit cube uniformly.

There is a second interesting observation that follows from [23]: Constraining the $g_j \bmod 2^m$ to be odd and unique for $0 \leq j < 2^{m-1}$ and $m \in \mathbb{N}$, obviously any first 2^{m-1} components $g_j \bmod 2^m$ are a permutation of all odd natural numbers less than 2^m . Simply selecting $g_j = 2j + 1$ does not result in good lattices, when the g_j are small with respect to b^m as explained above. In other words, finding a good generator vector is equivalent to reordering (or enumerating) the admissible components as mentioned in [23] and investigated in graphics [32].

Algorithm 4: Given pixel coordinates, `random_lattice` computes the selected component j of the i -th point of a rank-1 lattice sequence. The generator vector component is computed as a pseudo-random hash of the pixel position and component index. Note that the points are enumerated backwards to avoid sampling the common origin first. Ignoring the 32 most significant bits in the integer multiplication amounts to the mod 1 operation.

```
float random_lattice(uint32_t i, uint32_t j,
    uint32_t pixel_pos_x, uint32_t pixel_pos_y)
{
    uint32_t hash
        = hash_value(j, pixel_pos_x, pixel_pos_y);
    uint32_t lattice_param = hash | 1;

    uint32_t result = bit_reversal(0xFFFFFFFFu-i) // __brev
        * lattice_param; // backwards, to avoid 0
    return map_u32_to_unifloat(result);
}
```

2.4.2 Admissible Random Generator Vectors in Base $b = 2$

While good generator vectors do exist [16], there are no constructions in high dimensions and an exhaustive search is infeasible. For certain smoothness classes of functions, the component-by-component construction [2] has become practical. Interestingly, selecting generator vectors at random [29, 8] has shown quite good results. Such construction-free approaches avoid a computer search and lend themselves to problems that do not provide structure other than square integrability, like for example, light transport simulation.

As an example from computer graphics, Algorithm 4 determines the coordinate $x_i^{(j)}$ according to (2) by computing a hash value from the dimension j and the pixel coordinates in an image. Setting the least significant bit of the pseudo-random value yields the generator vector component g_j . Forcing the components to be odd

results in perfect stratification along each dimension for a base $b = 2$. This way, each pixel is assigned its own, pseudo-random rank-1 lattice sequence generator vector. Furthermore, the samples are enumerated backwards in order to avoid sampling with the origin as a common first sample across the screen, as this would result in aliasing rather than noise. Yet, the zero is not excluded [38] – it only comes last. The implementation is deterministic and hence reproducible. It does not access any lookup tables, which avoids any latency due to memory access.

As an alternative, the sequence of $g_j = 2\xi + 1$ may be generated by a pseudo-random number generator ξ , for example, a linear feedback shift register (LFSR) generator. The seed of the generator then defines the generator vector. Since $\xi = 0$ is not element of the LFSR sequence, a component with $g_j = 1$ can be added, which amounts to the radical inverse ϕ_2 in that dimension. As compared to [23], the algorithm uses only one LFSR instead of one per dimension and loads only one seed that determines the generator vector components computed on the fly without any further memory access. It is hence a highly desirable implementation on modern processors.

Creating an admissible random generator vector with unique components by using a pseudo-random number generator is simple. Guaranteeing uniqueness for the hash-based approach is tricky and in the extreme case requires computational verification. Another caveat is that it is not obvious how to enforce the criteria from the previous section when creating pseudo-random generator vectors. In a straightforward approach, one would skip pseudo-random numbers not fulfilling the criteria, which, for efficiency reasons, would require to tabulate the generator vectors.

2.5 Massive Parallelization

There are two key aspects of parallelization: Solving a large problem by parallel computation and solving a large number of problems in parallel. Quasi-Monte Carlo methods cover both aspects, are efficient in massively parallel heterogeneous computing environments, and in addition do not require intermediate synchronization.

Computing several millions of integrals simultaneously, 32-bit indices may not be sufficient. In addition, errors caused by an index wrapping around in 32 bits may be subtle and hard to find. It hence is important to be certain about the range of an index required by an application.

2.5.1 Partitioning Low Discrepancy Sequences

One approach to parallelization is to partition one low discrepancy sequence into multiple low discrepancy sequences and to assign each one subsequence to a processing element [25]. To do so, a low discrepancy sequence is extended by one dimension. The unit interval corresponding to the additional dimension is partitioned into the number P of processing elements. All points of the low discrepancy sequence whose

additional dimension is element of the p -th interval are assigned to the p -th processing element. For low discrepancy sequences based on radical inversion, the subsequences can be efficiently enumerated per processing element [25].

A second approach to massive parallelization has been developed for integro-approximation in computer graphics [12, 28]. In order to compute the color of each pixel in an image, a high-dimensional integral needs to be computed [41]. Using the first two dimensions of one high-dimensional low discrepancy sequence, the stratification imposed by the pixels in the image plane is used to assign each point of the low discrepancy sequence to exactly one pixel. Like before, the subsequence corresponding to one pixel can be efficiently enumerated for radical inversion based low discrepancy sequences.

Parallelization by partitioning low discrepancy sequences begins by assigning the subsequences to processing elements and ends with the reduction of the results. No intermediate communication is required. Since each processing element can enumerate its own subsequence, progressive and adaptive sampling can be controlled independently of the other processing elements.

Each part of the computation is deterministic and hence reproducible in principle. However, it is not always possible to control the exact order of additions in a massively parallel computing environment. This may introduce cancellation effects of random nature when repeating computations. To control this source of randomness, cancellation effects need to be kept at a minimum, for example by Kahan's algorithm, hierarchical reduction, sorting numbers before addition, or computation in integers, the last of which is truly commutative and associative as long as the results do not leave the integer range. A second caveat of the partitioning approach is that the number of required points in a massively parallel computation may easily exceed an index range representable within 32 bits. This can be resolved by using 64-bit integers for the indices, which comes at a certain cost, especially when 64-bit operations are emulated by 32 bit operations.

2.5.2 Randomized Quasi-Monte Carlo Methods

By randomizing one low discrepancy sequence [37, 30], each processing element may generate an individual low discrepancy sequence. This keeps the index range reasonable, even with massive parallelization. The reduction of the single results allows for an unbiased variance estimate, since all randomized sequences are independent. This comes at the price that the union of samples very unlikely is of low discrepancy, falling short with respect to maximum efficiency.

While this may be an issue when massively parallelizing one big problem, derandomized randomized quasi-Monte Carlo methods are an opportunity when computing many integrals in parallel as addressed in the next section on optimization.

2.6 Optimization

The algorithms for low discrepancy sequences based on radical inversion, generator matrices, and generator vectors share the property that once an efficient implementation is in place, the permutations and generators may be optimized and adapted to the actual application.

It has been recognized early on that random or randomized generator matrices [17] perform quite well and often better than the classic deterministic constructions [21]. Hence, instead of searching for better number-theoretic constructions, we may take advantage of the fact that many sets of random parameters are good and single out the bad ones. One such approach is to use the median of a number of randomized quasi-Monte Carlo integrations [9] that inspired investigations using random generator matrices [39] and random generator vectors [8].

In certain applications, the efficiency of using the median of repeated integration may be disputable and for this reason finding parameters by computer search remains an option. Minimizing the overall discrepancy and thus improving uniformity does not necessarily result in good low dimensional projections. This has been addressed in [19] for the Sobol' sequence and led to a more general framework to specify (t, m, s) -nets and (t, s) -sequences by constraints on projections [40]. This way, uniform point sets can be tailored to match lower-dimensional structures intrinsic to an integration problem. This is of advantage in finance and physics, where high-dimensional integrals often are composed of a sequence of low dimensional integrals. Similar tools exist for lattice rules [33].

Maximizing the minimum distance of point sets [21] is meaningful in small dimensions, especially in graphics. Corresponding experiments [11] even reveal the existence of (t, m, s) -nets that cannot be represented by (1). A related approach allows for designing a point set according to a desired energy spectrum [31]. While these approaches have benefits in two dimensions, they do not translate to efficient high-dimensional approaches.

Using higher bases and prime power bases in radical inversion (see Sec. 2.2) provides a larger design space for permutations and generator matrices. This is especially interesting to explore with computational scrambling.

When no means are at hand to assess the discrepancy of a point sequence, its quality may be inspected by integrating test functions. Many practical test functions have analytic integrals and are designed to be sensitive to irregularities of distribution when integrated numerically (for example, see [15, Sec.5.1]). Sometimes test functions are invariant to permutations of the dimensions, which, however, can make a difference in applications. As elaborated in Sec. 2.4.1 and explored in [32], assigning the dimensions of a low discrepancy sequence to the problem dimensions matters. This amounts to assigning the best uniformly distributed dimensions of a low discrepancy sequence to the most important dimensions of a problem. In practice, problems like light transport simulation typically act like a lens on the quality of low dimensional projections of a point sequence, as they reveal a lack of uniformity by exposing visual artifact structure in images.

2.6.1 Two Optimization Examples from Computer Graphics

Real-time graphics allows for only a very few samples per pixel to estimate its color. The resulting images likely look noisy and hence need to be filtered. Interestingly, the characteristic of the noise makes a difference. In fact, blue noise is most amenable to the human eye, as frequencies below the Shannon limit can be reproduced and frequencies above are mapped to noise, reducing distracting visible aliasing. This has been known for long, especially in computer graphics, however, only recently the focus shifted from blue noise properties of samples within a pixel to blue noise across the image plane [6].

Subsequent work has led to a very efficient implementation [13] that uses one low discrepancy sequence across all pixels and per-pixel randomization to achieve blue noise characteristics rather than aliasing: The tiny algorithm stores s -dimensional points $P = (p_1, \dots, p_N)$ of an Owen-scrambled Sobol' sequence (see Algorithm 3) as integers along with a digit scrambling table $s_{x,y}$ of $128^2 \times s$ integers and a scrambling table $r_{x,y}$ of 128^2 integers for reordering the points. Given the pixel coordinates $(x, y) \bmod 128$, the i -th sample is determined by

$$p_i^{(x,y)} = p_{i \oplus r_{x,y}} \oplus s_{x,y},$$

where \oplus is the bit-wise exclusive-or operation. The resulting integer $p_i^{(x,y)}$ is converted to floating point (see Algorithm 1). Both scrambling tables have been found by minimizing an energy functional by simulated annealing that yields the blue noise characteristics across the pixels.

Following these principles and inspecting the structure of light transport simulation by path tracing, an even simpler sampler [1] has been found shortly after. Tracing a light transport path consists of simulating a sequence of scattering events and visibility tests. The important observation is that aliasing will appear if at a certain bounce samples are correlated across pixels rather than along the whole path. Hence, to achieve blue noise properties, only one 128^2 table of two-dimensional shift vectors for Cranley-Patterson-rotations that is repeated for all pairs of dimensions is sufficient to decorrelate high-dimensional samples of one rank-1 lattice sequence with generator vectors from [15] across the pixels. The table of shifts has been computed by minimizing the variance across a set of test functions, where the loss has been determined after denoising the test images. Hence the shifts are already optimized with respect to noise filtering in mind.

As compared to the first example [13], the points of the rank-1 lattice sequence can be generated without a lookup table and the remaining lookup table for the Cranley-Patterson-rotations is small and low-dimensional, rendering its optimization much less complex [1]. Note that the design of the sampling algorithm is closely coupled to the structure of image synthesis by light transport simulation, i.e. the structure of the Neumann series to solve an integral equation.

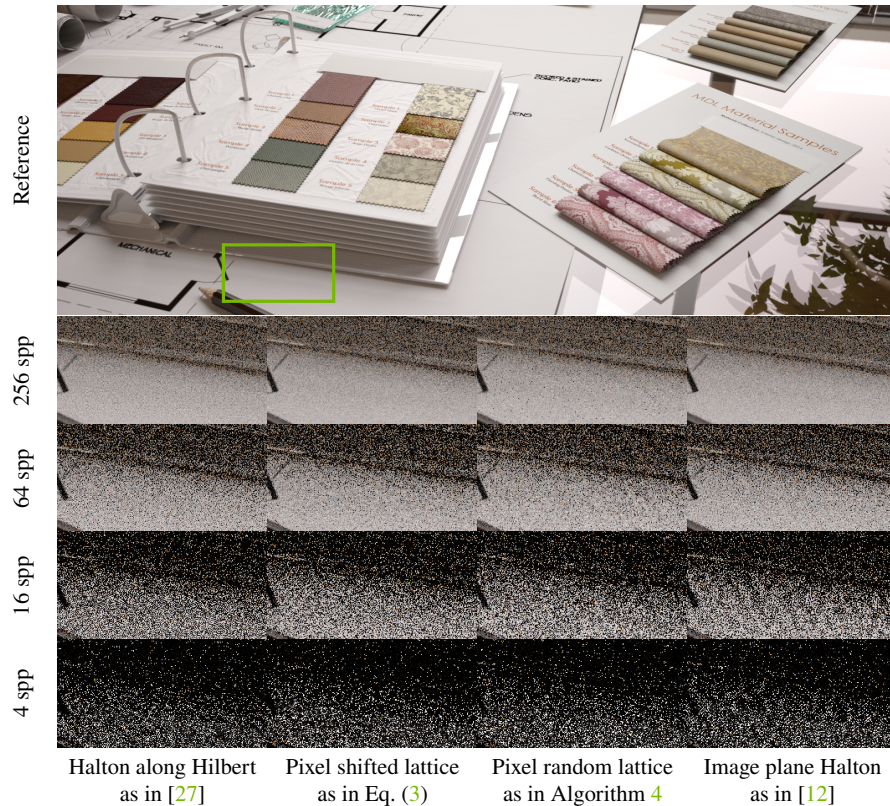


Fig. 1 Evolution of noise characteristics in light transport simulation at low number of samples per pixel (spp). The pixel shifted lattice as in Eq. (3) shows the overall best performance. At 256 spp, its noise is most uniform, has the least amount of black pixels, and does not expose structural correlation artifacts. Lacking guarantees on the quality of the generator vector, the pixel random lattices still show black pixels, exposing bad generator vectors. At low sampling rates, especially visible at 16 spp and 4 spp, the approaches using the Halton sequence expose axis-aligned structures, streaks, and ripples.

3 Results

With the teachings of the previous two examples from computer graphics, the question arises whether a similar reduction in the perceptual error can be achieved without optimization. In [27] multiple sampling algorithms have been introduced that take advantage of enumerating low discrepancy sequences along the Hilbert curve. In fact, they achieve characteristics similar to those of the desirable blue noise characteristics [6, 13, 1] without optimization.

In the following, we extend these investigations to new and simple algorithms based on rank-1 lattice sequences in base $b = 2$ as they only require three operations: bit reversal to compute ϕ_2 , multiplication, and mapping to floating point numbers in

the range $[0, 1)$ as shown in Algorithm 1. Fig. 1 compares the results of Algorithm 4 to prior work of enumerating a Halton sequence along the Hilbert curve over the image plane [27] and sampling the image plane by using the first two dimensions of a Halton sequence [12]. While the latter algorithms are consistent and hence convergent, at low sampling rates, the noise characteristics of the rank-1 lattice sequence algorithm outperform the image plane sampling approach. This is remarkable, as the extremely simple Algorithm 4 uses a pseudo-random generator vector per pixel and is more efficient to generate than the Halton sequence.

The outliers at 256 samples per pixel that become visible as salt-and-pepper noise are due to bad instances of the pseudo-random generator vectors. We find their number so small that a denoiser can remove them. As an alternative, already superimposing four instances of the random rank-1 lattice sequence in a pixel reliably hides the outliers, while remaining competitive in terms of performance. This favorably relates to removing outliers by a median [9, 39, 8].

Using one generator vector for all pixels, Belcour and Heitz [1] uncorrelated pixels by an optimized, padded low dimensional Cranley-Patterson-rotation table (see the previous section). In this paper, we propose the following, similar but new algorithm which does not require any optimization:

$$(\phi_2(i) + \phi_3(\text{inv_hilbert}(x, y))) \cdot g_j \bmod 1 \quad (3)$$

Instead of applying a single shift to each dimension of the rank-1 lattice sequence in Eq. (2), only one one-dimensional shift is applied to the radical inverse ϕ_2 before the generator vector multiplication. Drawing from prior work [27], we determine this one shift per pixel by enumerating the radical inverse ϕ_3 along the Hilbert curve in the image plane, where (x, y) are the pixel coordinates. This preserves the low discrepancy of the shifts across the pixel neighborhoods [7]. Selecting a co-prime radical inverse avoids interference with the radical inverse enumerating the points of the rank-1 lattice sequence. The implementation remains compact and simple: We tabulate one generator vector \mathbf{g} according to Sec. 2.4.1 and [23]. The radical inverse ϕ_2 is computed by bit reversal (see Algorithm 4), while the second radical inverse ϕ_3 is implemented using a small lookup table for the simultaneous inversion of four digits as shown in Algorithm 2 and derived in Sec. 2.2. The resulting code runs about 7 times faster than our previous approach [12], where we applied the linearly scrambled Halton sequence as in Algorithm 2, used permutation tables for the first 32 dimensions in combination with the simultaneous inversion of multiple digits, and replaced divisions and modulo operations by cheaper operations [43].

The pixel shifted lattice results in Fig. 1 compare well to the state of the art: At low sampling rates, they lack axis-aligned structures, streaks, and ripples of approaches using the Halton sequence. At higher sampling rates, the noise characteristics are most uniform and avoid the failure cases inherent with randomly selected generator vectors. For typical use cases with 200-2000 samples per pixel and for scenes with contemporary geometric complexity, sampling according to Eqn. (3) has been extremely robust while still exhibiting the desirable noise characteristics across sampling rates and almost minimal code complexity.

4 Conclusion

We present quasi-Monte Carlo algorithms for radical inversion, digital nets and sequences, and rank-1 lattice sequences as they are implemented in industry for reasons of efficiency, precision, and robustness. With a focus on rank-1 lattice sequences, current and future optimizations of low discrepancy sequences have been discussed. Along these lines, a new improved sampling algorithm for image synthesis has been introduced. Although developed in the context of massively parallel light transport simulation, the techniques in this paper have applications not only in computer graphics software. An avenue of future research is crafting low discrepancy sequences according to the intrinsic structure of integro-approximation problems [40].

References

1. Belcour, L., Heitz, E.: Lessons learned and improvements when building screen-space samplers with blue-noise error distribution. CoRR **abs/2105.12620** (2021). URL <https://arxiv.org/abs/2105.12620>
2. Cools, R., Kuo, F., Nuyens, D.: Constructing embedded lattice rules for multivariate integration. SIAM Journal on Scientific Computing **28**, 2162–2188 (2006)
3. Downey, A.B.: Generating pseudo-random floating-point values (2007). URL <https://alldowney.com/research/rand/>. <https://alldowney.com/research/rand/>
4. Faure, H.: Good permutations for extreme discrepancy. J. Number Theory **42**, 47–56 (1992)
5. Faure, H., Lemieux, C.: Generalized Halton sequences in 2008: A comparative study. ACM Transactions on Modeling and Computer Simulation **19**(4), 15:1–15:31 (2009)
6. Georgiev, I., Fajardo, M.: Blue-noise dithered sampling. ACM SIGGRAPH 2016 Talks (2016)
7. Gerber, M., Chopin, N.: Sequential quasi-Monte Carlo. Journal of the Royal Statistical Society. Series B (Statistical Methodology) **77**(3), 509–579 (2015). URL <http://www.jstor.org/stable/24774819>
8. Goda, T., L’Ecuyer, P.: Construction-free median quasi-Monte Carlo rules for function spaces with unspecified smoothness and general weights. SIAM Journal on Scientific Computing **44**(4), A2765–A2788 (2022). DOI 10.1137/22M1473625. URL <https://doi.org/10.1137/22M1473625>
9. Goda, T., Suzuki, K.: A universal median quasi-Monte Carlo integration. arXiv **0**(0), 0–0 (2022). URL <https://arxiv.org/pdf/2209.13186.pdf>
10. Goldberg, D.: What every computer scientist should know about floating-point arithmetic. ACM Computing Surveys **23**(1), 5–48 (1991)
11. Grünschloß, L., Keller, A.: (t, m, s) -nets and maximized minimum distance, Part II. In: P. L’Ecuyer, A. Owen (eds.) Monte Carlo and Quasi-Monte Carlo Methods 2008, pp. 395–409. Springer (2009). URL <http://gruenschloss.org/diag0m2/diag0m2.pdf>
12. Grünschloß, L., Raab, M., Keller, A.: Enumerating quasi-Monte Carlo point sequences in elementary intervals. In: L. Plaskota, H. Woźniakowski (eds.) Monte Carlo and Quasi-Monte Carlo Methods 2010, pp. 399–408. Springer (2012). URL <http://gruenschloss.org/sample-enum/sample-enum.pdf>
13. Heitz, E., Belcour, L., Ostromoukhov, V., Coeurjolly, D., Iehl, J.C.: A low-discrepancy sampler that distributes Monte Carlo errors as a blue noise in screen space. In: SIGGRAPH’19 Talks. ACM, Los Angeles, United States (2019). URL <https://hal.archives-ouvertes.fr/hal-02150657>

14. Hickernell, F., Hong, H., L'Ecuyer, P., Lemieux, C.: Extensible lattice sequences for quasi-Monte Carlo quadrature. *SIAM J. Sci. Comput.* **22**, 1117–1138 (2001)
15. Hickernell, F.J., Kritzer, P., Kuo, F.Y., Nuyens, D.: Weighted compound integration rules with higher order convergence for all N . *Numerical Algorithms* **59**, 161–183 (2012). URL <https://doi.org/10.1007/s11075-011-9482-5>
16. Hickernell, F.J., Niederreiter, H.: The existence of good extensible rank-1 lattices. *Journal of Complexity* **19**, 286–300 (2003)
17. Hong, H.S.: Digital Nets and Sequences for Quasi-Monte Carlo Methods. Ph.D. thesis, Hong Kong Baptist University (2002)
18. Joe, S., Kuo, F.: Remark on algorithm 659: Implementing Sobol's quasirandom sequence generator. *ACM Trans. Math. Softw.* **29**(1), 49–57 (2003)
19. Joe, S., Kuo, F.: Constructing Sobol' sequences with better two-dimensional projections. *SIAM Journal on Scientific Computing* **30**(5), 2635–2654 (2008)
20. Joe, S., Kuo, F.: Notes on generating Sobol' sequences. Technical report, School of Mathematics and Statistics, University of New South Wales (2008). URL <http://web.maths.unsw.edu.au/~fkuo/sobol/joe-kuo-notes.pdf>
21. Keller, A.: Myths of computer graphics. In: H. Niederreiter (ed.) *Monte Carlo and Quasi-Monte Carlo Methods 2004*, pp. 217–243. Springer (2006)
22. Keller, A.: Quasi-Monte Carlo image synthesis in a nutshell. In: J. Dick, F. Kuo, G. Peters, I. Sloan (eds.) *Monte Carlo and Quasi-Monte Carlo Methods 2012*, pp. 203–238. Springer (2013)
23. Keller, A., Binder, N., Wächter, C.: Construction of a rank-1 lattice sequence based on primitive polynomials. In: G. Larcher, F. Pillichshammer, A. Winterhof, C. Xing (eds.) *Applied Algebra and Number Theory*, pp. 204–215. Cambridge University Press (2014). DOI 10.1017/CBO9781139696456.013
24. Keller, A., Georgiev, I., Ahmed, A., Christensen, P., Pharr, M.: My favorite samples. In: *ACM SIGGRAPH 2019 Courses, SIGGRAPH '19*, pp. 15:1–15:271. ACM, New York, NY, USA (2019). DOI 10.1145/3305366.3329901. URL <http://doi.acm.org/10.1145/3305366.3329901>
25. Keller, A., Grünschloß, L.: Parallel quasi-Monte Carlo integration by partitioning low discrepancy sequences. In: L. Plaskota, H. Woźniakowski (eds.) *Monte Carlo and Quasi-Monte Carlo Methods 2010*, pp. 487–498. Springer (2012). URL <http://gruenschloß.org/parqmc/parqmc.pdf>
26. Keller, A., Premože, S., Raab, M.: Advanced (quasi) Monte Carlo methods for image synthesis. In: *ACM SIGGRAPH 2012 Courses, SIGGRAPH '12*. Association for Computing Machinery, New York, NY, USA (2012). DOI 10.1145/2343483.2343502. URL <https://doi.org/10.1145/2343483.2343502>
27. Keller, A., Wächter, C., Binder, N.: Rendering along the Hilbert curve. In: Z. Botev, A. Keller, C. Lemieux, B. Tuffin (eds.) *Advances in Modeling and Simulation: Festschrift for Pierre L'Ecuyer*, pp. 319–332. Springer (2022)
28. Keller, A., Wächter, C., Raab, M., Seibert, D., Antwerpen, D., Korndörfer, J., Kettner, L.: The Iray light transport simulation and rendering system. *CoRR* **abs/1705.01263** (2017). URL <http://arxiv.org/abs/1705.01263>
29. Kritzer, P., Kuo, F.Y., Nuyens, D., Ullrich, M.: Lattice rules with random n achieve nearly the optimal $O(n^{-\alpha-1/2})$ error independently of the dimension. *Journal of Approximation Theory* **240**, 96–113 (2019)
30. L'Ecuyer, P., Lemieux, C.: Recent Advances in Randomized quasi-Monte Carlo methods. In: M. Dror, P. L'Ecuyer, F. Szidarovszky (eds.) *Modeling Uncertainty: An Examination of Stochastic Theory, Methods, and Applications*, pp. 419–474. Kluwer Academic Publishers (2002)
31. Leimkühler, T., Singh, G., Myszkowski, K., Seidel, H.P., Ritschel, T.: Deep point correlation design. *ACM Trans. Graph.* **38**(6) (2019). DOI 10.1145/3355089.3356562. URL <https://doi.org/10.1145/3355089.3356562>

32. Liu, H., Han, H., Jiang, M.: Rank-1 lattices for efficient path integral estimation. *Computer Graphics Forum* **40**(2), 91–102 (2021). DOI <https://doi.org/10.1111/cgf.142617>. URL <https://onlinelibrary.wiley.com/doi/abs/10.1111/cgf.142617>
33. L'Ecuyer, P., Marion, P., Godin, M., Puchhammer, F.: A tool for custom construction of QMC and RQMC point sets. In: *International Conference on Monte Carlo and Quasi-Monte Carlo Methods in Scientific Computing*, pp. 51–70. Springer (2022)
34. Maize, E.: *Contributions to the Theory of Error Reduction in Quasi-Monte Carlo Methods*. Ph.D. thesis, The Claremont Graduate School (1980)
35. Maize, E., Sepikas, J., Spanier, J.: Accelerating the convergence of lattice methods by importance sampling-based transformations. In: L. Plaskota, H. Woźniakowski (eds.) *Monte Carlo and Quasi-Monte Carlo Methods 2010, Springer Proceedings in Mathematics & Statistics*, vol. 23, pp. 557–572. Springer (2012)
36. Niederreiter, H.: *Random Number Generation and Quasi-Monte Carlo Methods*. SIAM, Philadelphia (1992)
37. Owen, A.B.: Monte Carlo extension of quasi-Monte Carlo. In: *Proceedings of the 1998 Winter Simulation Conference*, pp. 571–577. IEEE Press (1998)
38. Owen, A.B.: On dropping the first Sobol' point. In: A. Keller (ed.) *Monte Carlo and Quasi-Monte Carlo Methods 2020*, pp. 71–86. Springer International Publishing, Cham (2022)
39. Pan, Z., Owen, A.B.: Super-polynomial accuracy of one dimensional randomized nets using the median-of-means. *Mathematics of Computation* **0**(0), 0–0 (2022). URL <https://arxiv.org/abs/2111.12676>
40. Paulin, L., Coeurjolly, D., Bonneel, N., Iehl, J.C., Keller, A., Ostromoukhov, V.: MatBuilder: Mastering sampling uniformity over projections. *ACM Transactions on Graphics* **41**(4), 84:1–84:13 (2022)
41. Pharr, M., Jacob, W., Humphreys, G.: *Physically Based Rendering - From Theory to Implementation*. Morgan Kaufmann, fourth edition (2023)
42. Walker, A.J.: Fast generation of uniformly distributed pseudorandom numbers with floating-point representation. *Electronics Letters* **10**, 533–534 (1974)
43. Warren, H.S.: *Hacker's Delight*. Pearson Education (2012). URL <https://books.google.de/books?id=VicPJYM0I5QC>